Supplemental Information

For Liu, Huang et al.: "Time-resolved proteomics vs. ribosome profiling reveals translation dynamics under stress"

Contents:

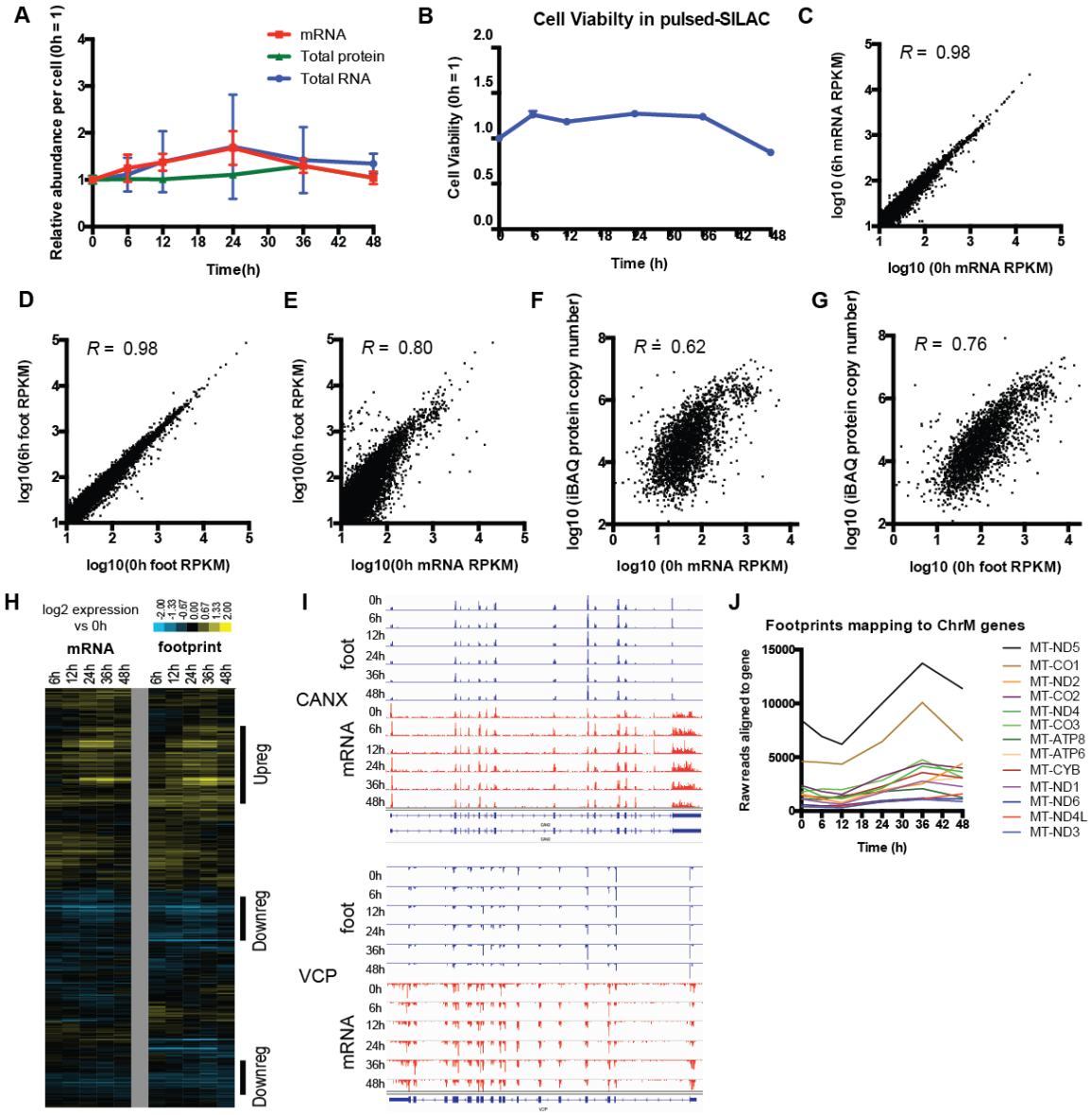

Figure S1. Biochemical changes after bortezomib treatment and comparison of baseline deep sequencing and proteomic data. Related to Figure 1 and Figure 2. A. Total RNA, mRNA, and protein per cell show little change during the time course after low-dose bortezomib treatment. Values +/- S.D. measured in biological quadruplicate and normalized to cell viability data at each time point to determine concentration per cell. **B.** Low-dose bortezomib treatment with heavy SILAC media pulse also reflects similar response to drug at level of cell viability as compared to non-SILAC media (Figure 1B). Values +/- S.D. measured in technical duplicate. **C-E.** Correlation between normalized read density (in RPKM) across 5642 transcripts with a minimum RPKM = 10 mapping to each gene, per the Ribomap algorithm (STAR Methods), comparing 0h and 6h mRNA-seq datasets (**C**), 0h and 6h ribosome footprint datasets (**D**), and 0h mRNA and 0h ribosome footprint datasets (**E**). **F-G**. Correlation between baseline ribosome footprint read density (**F**) and mRNA-seq read density (**G**) with estimated protein copy number per cell, with values averaged from duplicate iBAQ analysis (STAR Methods). **H.** Heatmap comparing mRNA-seq and ribosome footprint coding sequence read density (in RPKM) across all included transcripts. "Upreg" and "Downreg" clusters used for analysis in Dataset S2. **I.** Raw aligned ribosome footprint and mRNA-seq reads for two example proteins monitored by SRM assay (CANX and VCP). Note that footprint reads only map to coding exons (noted as thick bars in blue track at bottom of each panel; medium bars are untranslated regions; thin bars are intronic or intergenic) whereas mRNA-seq reads also map to 5' and 3' untranslated regions. Direction of reads reflects gene encoding on plus (reads directed up) or minus (reads

directed down) strand of genome. Screenshot from Integrative Genomics Viewer. **J.** Ribosome footprint reads across the time course mapping to ChrM. Increased ChrM mapping reads across the time course are consistent with decreased cytosolic ribosomal translation (Iwasaki et al., 2016).

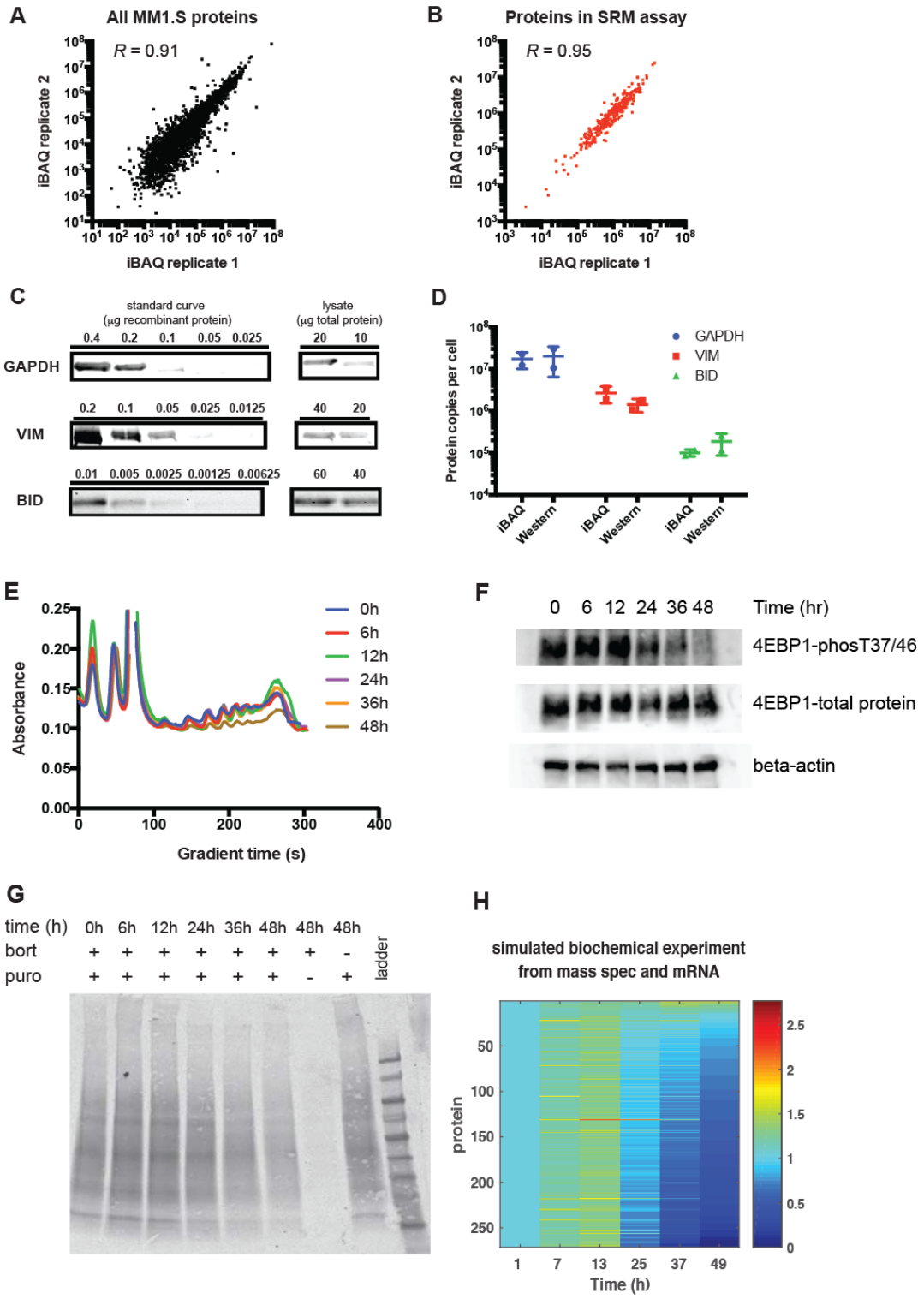

Figure S2. iBAQ estimation of protein copies per cell at baseline and changes in global translation across time course. Related to Figure 3. A. Baseline protein copy numbers per cell estimated using iBAQ are largely consistent across two biological replicates in MM1.S cells (n = 2704 protein groups with iBAQ estimate in both replicates). **B.** Proteins monitored by SRM assay (n = 272) show high reproducibility in baseline quantification based on iBAQ data. **C.** Quantitative Western blot data for three

high-abundance example proteins. **D.** Comparison of iBAQ and quantitative Western blot data for independent biological replicates suggests iBAQ provides similar estimates for high-abundance proteins. Error bars show mean +/- S.D. **E.** Polysome profiles obtained by sucrose gradient ultracentrifugation indicate diminishment of translation at the end of the time course. **F.** Western blot shows eIF4E Binding Protein-1 (4EBP1) dephosphorylation after low-dose bortezomib treatment, consistent with general translational inhibition. **G.** Puromycin incorporation into nascent protein chains (1-hr pulse of puromycin added at each time point prior to cell harvest; Western blot with anti-puromycin antibody) demonstrates decreased global protein synthesis at later time points. **H.** Simulation of protein abundance using the differential equation we proposed with the derived mRNA abundance $M_g(t)$, degradation rate constant k_g^d and translational rate parameter $k_g^s(t)$. At each sampling time τ we simulated the protein abundance after one hour with the initial conditions that the protein abundance at τ was 0. The heatmaps were normalized by the first column to show the relative abundance.

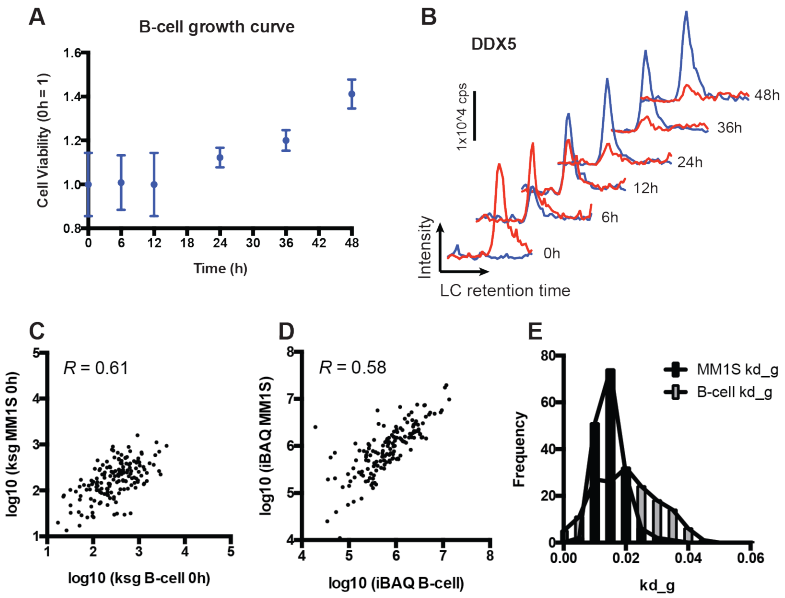

Figure S3. Extension of quantitative model to additional dataset in EBV-immortalized B-cells. Related to Figure 4. A. Growth of EBV-immortalized B-cells over the untreated time course (CellTiterGlo reagent; technical triplicate at each time point +/- S.D.) **B.** Example pSILAC targeted proteomic data for peptide from protein DDX5 shows similar kinetics of synthesis and degradation as in MM1.S (Fig. 2A). Blue = newly synthesized across time course, red = degraded from baseline. Similar correlations between (**C**) $k_g^s(0)$ as well as (**D**) iBAQ values in MM1.S and EBV B-cells for the proteins included in both SRM assays. **E.** Comparison of protein degradation rate constants k_g^d for proteins monitored in both cell lines suggests that low-dose bortezomib treatment in MM1.S leads to a decrease in degradation rate for some proteins.

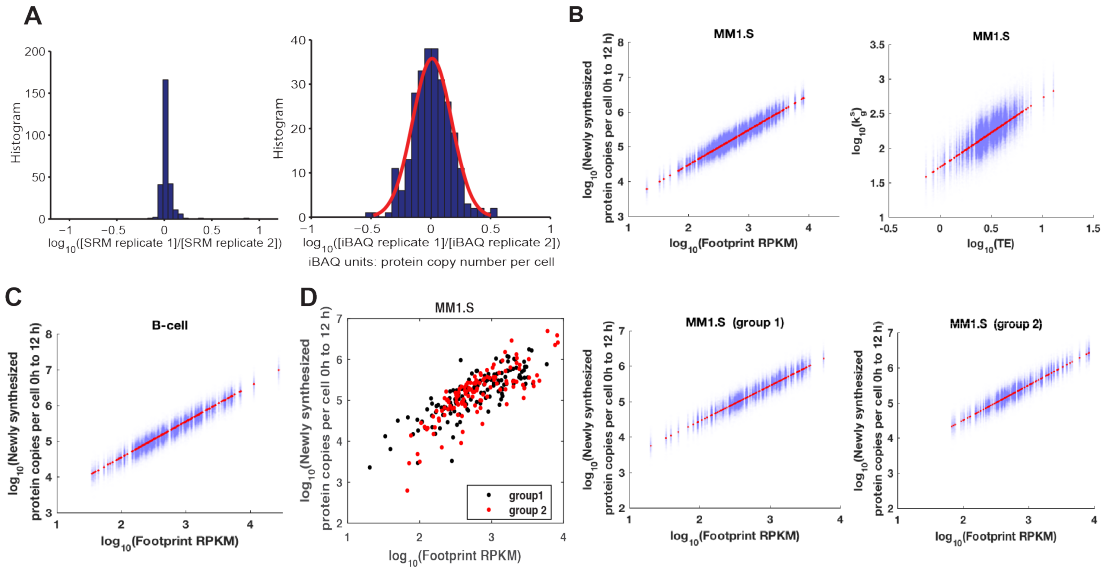

Figure S4. Error modeling based on iBAQ values and transcript-level isoforms. Related to Figure 4. **A.** MM1.S data demonstrates strong reproducibility for SRM replicate intensity but increased variance in iBAQ absolute copy number replicates. **B.** A gene specific scaling factor s_g is randomly generated according to the fitted normal distribution of the differences between the log-transformed iBAQ replicates (red curve in **A**, *right*) to simulate the effect of iBAQ noise. These simulated iBAQ values are used to generate point clouds of newly synthesized proteins per cell measured by SRM intensity as in Fig 3A and Fig 3D for MM1.S. Compared to the distributions in Fig 3A and Fig 3D, the iBAQ noise explained 36% and 10% of the deviation from the linear regression fits, respectively. **C.** Compared to the distribution in Fig 4A for B-cells, the iBAQ noise explained 23% of the deviation from the linear regression fits. **D.** All 272 protein-transcript pairs monitored in MM1.S cells were sorted into two groups. Group 1: One dominant transcript isoform (>80% of RNA-seq read density on a single isoform, per paired-end RNA-seq analysis at www.keatslab.org/data-repository/HMCL66_Transcript_Expression_FPKM.xlsx) (n =145). Group 2: No dominant transcript isoform (n = 127). The iBAQ noise explained 47% and 35% of the deviation from the linear regression fits for group 1 and group 2 respectively.

Upreg	*Category*	*Term*	*p-value*
	GOTERM_CC_DIRECT	GO:0000502~proteasome complex	3.07E-48
	UP_KEYWORDS	Proteasome	1.21E-46
	KEGG_PATHWAY	hsa03050:Proteasome	1.04E-35
	GOTERM_BP_DIRECT	GO:0006521~regulation of cellular amino acid metabolic process	6.37E-35
	GOTERM_BP_DIRECT	GO:0051437~positive regulation of ubiquitin-protein ligase activity involved in regulation of mitotic cell cycle transition	1.34E-33
Downreg			
	GOTERM_BP_DIRECT	GO:0006614~SRP-dependent cotranslational protein targeting to membrane	1.61E-16
	GOTERM_BP_DIRECT	GO:0006413~translational initiation	1.34E-15
	GOTERM_BP_DIRECT	GO:0019083~viral transcription	6.88E-14
	UP_KEYWORDS	Ribosomal protein	7.24E-13
	KEGG_PATHWAY	hsa03010:Ribosome	1.21E-12

Table S1. Biological processes in Upreg and Downreg transcripts in response to bortezomib treatment. Most enriched results from DAVID analysis (32) with default settings and human as species. Top five most enriched terms shown measured from "Upreg" and "Downreg" clusters, as in Figure S1H.

	Performance measure	Translational rate parameter $k_g^s(t)$	Protein synthesis rate
Replicates	correlation coefficient	0.8312	0.8202
	RMAE	0.1549	0.1259
Estimation	correlation coefficient	0.8788	0.8801
	RMAE	0.4406	0.3420
Prediction	correlation coefficient	0.8684	0.9000
	RMAE	0.1609	0.2079

Table S2. Estimation and prediction of translational rate parameter $k_g^s(g)$ and protein synthesis rates. The Pearson correlation coefficient and relative mean absolute error (RMAE) of the estimation and prediction of translational rate parameter and protein synthesis rate averaged over all the genes were compared to those between the two mass spectrometry replicates We define the relative mean absolute error between two time series $f_1\ (t)$ and $f_2\ (t)$ as $\frac{1}{T}\int_0^T |f_1\ (t) - f_2\ (t))|/|f_2\ (0)|dt$.

Key Resources Table

REAGENT or RESOURCE	SOURCE	IDENTIFIER
Antibodies		
Rabbit monoclonal anti-GAPDH	Cell Signaling Technology	Cat# 2118L
Rabbit monoclonal anti-vimentin	Cell Signaling Technology	Cat# 5741P
Rabbit polyclonal anti-Bid	Cell Signaling Technology	Cat# 2002P
Mouse monoclonal anit-puromycin	KeraFast	Cat# 3RH11
Rabbit monoclonal anti-4E-BP1	Cell Signaling Technology	Cat# 53H11
Rabbit monoclonal anti-phospho-4E-BP1 (T37/46)	Cell Signaling Technology	Cat# 236B4
Chemicals, Peptides, and Recombinant Proteins		
Bortezomib	LC Laboratories	B-1408
Cycloheximide	Sigma-Aldrich	Cat# C4859; CAS: 66-81-9
L-Lysine 4,4,5,5-D4 (Lys4)	Cambridge Isotope Laboratories	Cat# DLM-2640
L-Arginine $^{13}C_6$ (Arg6)	Cambridge Isotope Laboratories	Cat# CLM-2265-H
L-Lysine $^{13}C_6{}^{15}N_2$ (Lys8)	Cambridge Isotope Laboratories	Cat# CNLM-291-H
L-Lysine $^{13}C_6{}^{15}N_4$ (Arg10)	Cambridge Isotope Laboratories	Cat# CNLM-593-H
L-Lysine	Sigma-Aldrich	Cat# 8662; CAS: 657-27-2
L-Arginine	Sigma-Aldrich	Cat# A6969; CAS: 1119-34-2
TRIzol® reagent	Life Technologies	Cat# 15596026
HALT protease and phosphatase inhibitor single use cocktail	Thermo Fisher	Cat# 78443
Sequencing Grade Modified Trypsin	Promega	Cat# V5111
GAPDH recombinant protein	Abcam	Cat# ab82633
Vimentin recombinant protein	PeptroTech	Cat# 110-10
Bid recombinant protein	Sino Biological	Cat# 10468-HNCE-59
Critical Commercial Assays		
Rneasy mini kit	QIAgen	Cat# 74104
Quantifluor RNA assay	Promega	Cat# E3310
Oligo(dT)25 Magnetic Beads kit	New England BioLabs	Cat# S1419S
Pierce™ BCA Protein Assay Kit	Thermo Fisher Scientific	Cat# 23225
SepPak C18 columns	Waters	Cat# WAT020515
CellTiter-Glo® Luminescent Cell Viability Assay	Promega	Cat# G7570
Caspase-Glo® 3/7 Assay Systems	Promega	Cat# G8090
Invitrogen MyOne streptavidin C1 dynabeads	Thermo Fisher	Cat# 65001
Experimental Models: Cell Lines		
MM.1S	ATCC	Cat# CRL-2974
EBV-transformed B-cell	Markus Muschen (University of California San Francisco, USA)	N/A
Sequence-Based Reagents		

miRNA Cloning Linker 1 DNA oligo: 5' AppCTGTAGGCACCATCAAT/3ddC 3'	IDT	N/A
rRNA subtraction DNA oligo oNTI309: (biotin)-TCCTCCCGGGGCTACGCCTGTCTGAGCGTCGCT	IDT	N/A
rRNA subtraction DNA oligo oNTI301r : (biotin)-GGGCCTCGATCAGAAGGACTTGGGCCCCCCACGA	IDT	N/A
rRNA subtraction DNA oligo oNTI305r : (biotin)-GGCGAGACGGGCCGGTGGTGCGCCCTCGGCGGA	IDT	N/A
rRNA subtraction DNA oligo oNTI307hr : (biotin)-GCGGGGGACCGGCTATCCGAGGCCAACCGAGGCTC	IDT	N/A
rRNA subtraction DNA oligo oNTI298r : (biotin)-TGATCTGATAAATGCACGCATCCCCCC	IDT	N/A
rRNA subtraction DNA oligo oNTI303hr : (biotin)-CGCGCCGTGGGAGGGGTGGCCCGGCCCC	IDT	N/A
Rev Transcription DNA oligo oNTI225-Link1 (DNA): 5'/5Phos/GATCGTCGGACTGTAGAACTCTGAACCTGTC GGTGGTCGCCGTATCATT/iSp18/CACTCA/iSp18/CAAG CAGAAGACGGCATACGAATTGATGGTGCCTACAG 3'	IDT	N/A
Amplification DNA primer oNTI230 (DNA): 5′ - AATGATACGGCGACCACCGA	IDT	N/A
Amplification DNA primer oNTI231 (DNA): 5′ - CAAGCAGAAGACGGCATACGA	IDT	N/A
Software and Algorithms		
MaxQuant v1.5.1.2	Cox and Mann, 2008	http://www.biochem.mpg.de/5111795/maxquant
Skyline v2.5	MacLean *et al*., 2010	https://skyline.ms/project/home/software/Skyline/begin.view
Ribomap	Wang *et al*., 2016	https://github.com/Kingsford-Group/ribomap
Star v.2.4.0j	Dobin *et al.*, 2012	https://github.com/alexdobin/STAR/releases/tag/STAR_2.4.0j
Cluster 3.0	de Hoon *et al*., 2004	http://bonsai.hgc.jp/~mdehoon/software/cluster/software.htm
Java TreeView	Saldanha, A.J. 2004	httP://jtreeview.sourceforge.net
DAVID Bioinformatics Resource	Huang *et al*., 2009	http://david.ncifcrf.gov
MATLAB R2013a	Mathworks	http://www.mathworks.com/products/matlab/
MATLAB spline fit script	This paper	https://sourceforge.net/projects/ncspline/
Other		